



Full Text View

[Volume 32, Issue 9 \(September 2002\)](#)

Journal of Physical Oceanography

Article: pp. 2541–2558 | [Abstract](#) | [PDF \(647K\)](#)

On Determining the Onset and Strength of Breaking for Deep Water Waves. Part I: Unforced Irrotational Wave Groups

Jin-Bao Song and Michael L. Banner

School of Mathematics, The University of New South Wales, Sydney, New South Wales, Australia

(Manuscript received June 26, 2001, in final form January 14, 2002)

DOI: 10.1175/1520-0485(2002)032<2541:ODTOAS>2.0.CO;2

ABSTRACT

Finding a robust threshold variable that determines the onset of breaking for deep water waves has been an elusive problem for many decades. Recent numerical studies of the unforced evolution of two-dimensional nonlinear wave trains have highlighted the complex evolution to recurrence or breaking, together with the fundamental role played by nonlinear intrawave group dynamics. In Part I of this paper the scope of two-dimensional nonlinear wave group calculations is extended by using a wave-group-following approach applied to a wider class of initial wave group geometries, with the primary goal of identifying the differences between evolution to recurrence and to breaking onset. Part II examines the additional influences of wind forcing and background shear on these evolution processes.

The present investigation focuses on the long-term evolution of the maximum of the local energy density along wave groups. It contributes a more complete picture, both long-term and short-term, of the approach to breaking and identifies a dimensionless local average growth rate parameter that is associated with the mean convergence of wave-coherent energy at the wave group maximum. This diagnostic growth rate appears to have a common threshold for all routes to breaking in deep water that have been examined and provides an earlier and more decisive indicator for the onset of breaking than previously proposed breaking thresholds. The authors suggest that this growth rate may also provide an indicative measure of the strength of wave breaking events.

1. Introduction

Wave group structure has been a conspicuous feature of ocean wave height records ever since such measurements have

Table of Contents:

- [Introduction](#)
- [Details of numerical](#)
- [Properties of nonlinear](#)
- [Scope of the present](#)
- [Results](#)
- [Conclusions](#)
- [REFERENCES](#)
- [APPENDIX](#)
- [TABLES](#)
- [FIGURES](#)

Options:

- [Create Reference](#)
- [Email this Article](#)
- [Add to MyArchive](#)
- [Search AMS Glossary](#)

Search CrossRef for:

- [Articles Citing This Article](#)

Search Google Scholar for:

- [Jin-Bao Song](#)
- [Michael L. Banner](#)

been available. Within these evolving wave groups, very steep waves arise intermittently and can represent a serious hazard to shipping and offshore structures, especially if they break. Insightful observational contributions linking wave breaking and wave group structure were made by [Donelan et al. \(1972\)](#) and subsequently by [Holthuijsen and Herbers \(1986\)](#). While the most popular description of wind-generated ocean waves has been in terms of the wave height spectrum, a significant literature also exists on the statistics of wave groups, wave heights, and associated propagation characteristics. The review articles by [Donelan and Hui \(1990\)](#), [Banner and Peregrine \(1993\)](#), and [Melville \(1996\)](#) provide complementary surveys of the recent literature on the time-honored problem of wave breaking in deep water.

Of particular relevance to the discussion of wind-forced waves and the statistics and structure of extreme waves in wave groups are the papers of [Longuet-Higgins \(1984\)](#), [Boccotti et al. \(1993\)](#), [Phillips et al. \(1993\)](#), and [Osborne et al. \(2000\)](#), among others. These papers, however, do not address the underlying issue of determining the onset of wave breaking. With the availability of elegant analytic methods, there has been a strong ongoing interest in studying nonlinear modulational processes in model equations such as the nonlinear Schrödinger equation and its higher order variants (e.g., [Dysthe 1979](#)). [Dias and Kharif \(1999\)](#) provide a particularly insightful review of the impressive mathematical progress with these equations. While well suited to examining many aspects of this problem, these model equations are not able to describe the onset of wave breaking, which requires the exact Euler equation formulation with fully nonlinear free surface boundary conditions. While it is recognized that wave breaking is characteristically three-dimensional (3D), modeling and measurements of two-dimensional (2D) breaking are somewhat less demanding and such 2D studies have provided valuable insight into the breaking process.

A number of authors have contributed recent 2D numerical investigations on wave breaking onset, including [Dold and Peregrine \(1986\)](#), [Tulin and Li \(1992\)](#), [Griffin et al. \(1996\)](#), and [Banner and Tian \(1998\)](#), among others. Typically, these studies are valid up to the point of crest overturning. Complementary observational investigations have been reported on the unforced (zero wind) case by a number of authors, including [Melville \(1982, 1983\)](#), [Rapp and Melville \(1990\)](#), [Kway et al. \(1998\)](#), and [Tulin and Waseda \(1999\)](#). Valuable observational insight has been provided for the extension to 3D breaking by [Nepf et al. \(1998\)](#). While each of these studies has provided new insight into the complexity of the breaking onset and its postbreaking transition, key issues and questions still remain.

Our present investigation focuses on (a) determinants of breaking onset, (b) how far in advance wave breaking events can be predicted, and (c) what determines their strength. It refines and extends significantly the numerical study of [Banner and Tian \(1998\)](#), henceforth referred to as BT), who investigated the onset of wave breaking for a particular class of unforced modulating wave groups of nonlinear deep water surface gravity waves. BT also provide a detailed overview of the background literature of the unforced problem.

Briefly, BT used the fully nonlinear two-dimensional, periodic domain inviscid model developed by [Dold and Peregrine \(1986\)](#), henceforth referred to as DP). Dold and Peregrine, and subsequently BT, discuss the two diverse modes of evolution of the class of unforced two-dimensional nonlinear modulating wave groups with a central carrier wave of moderate initial steepness and two small symmetric sidebands. The deforming wave group evolves either with recurrence to the original wave group structure or to breaking. For this class of initial wave group structure (designated case I and described in detail below), Dold and Peregrine reported that an initial carrier wave steepness threshold determines which of these evolution modes occurs. In this paper, we revisit case I and, in order to examine the sensitivity to initial conditions for this highly nonlinear problem, have also included a parallel study of the behavior of two other classes of initial wave group geometry. Case II consists of two equal, moderately steep wave components with slightly different frequencies. The inclusion study of a third class (designated case III), known as a “chirped” wave packet, was motivated by its widespread use as the preferred laboratory wave tank method for the controlled generation of breaking waves, for example, [Rapp and Melville \(1990\)](#), henceforth referred to as RM).

Using the numerical models described in [section 2](#) below, typical evolution results for these three cases are visualized in [Figs. 1](#) and [2](#). [Figure 1](#) shows the evolution to recurrence for an initial wave group for an example of each of the three cases just below the recurrence threshold. [Figure 2](#) shows the evolution to breaking just above the recurrence threshold. At this point, a measure of initial steepness is used to differentiate the two distinct evolution behaviors. To emphasize the fundamental role of nonlinear energy fluxes occurring within wave groups in each of these evolutions, [Figs. 1](#) and [2](#) also show the corresponding behavior of the local depth-integrated energy density (potential plus kinetic) associated with the motion. One striking common feature is immediately apparent: for either breaking or recurrence, the evolution is accompanied by a systematic *mean convergence* of the energy density toward the local maximum of the evolving wave group.

It is observed that individual waves break with varying strengths, ranging from “gently spilling” to “strongly plunging.” In a pioneering laboratory study aimed at elucidating the issue of strength of breaking events, RM introduced an effective relative energy loss parameter as the change in wave packet energy density (energy per unit width of the flow for 2D waves) normalized by the energy density prior to breaking. They explored systematically how this parameter varied as a function of their initial wave steepness parameter ak_c (defined in [section 3a](#)) for wave packets with different properties such as relative bandwidth, center frequency, wave packet propagation distance to breaking, etc. We propose below that the trend

of the energy loss behavior observed by RM is linked to the systematic mean convergence rate of the energy density toward the local maximum of the evolving wave group.

2. Details of numerical approach

a. Nonlinear wave codes and their numerical accuracy

We used the fully nonlinear, two-dimensional, periodic domain inviscid model for free surface gravity water waves described in detail in DP. In this model, the following scalings were used: gravitational acceleration $g = 1$, water density $\rho_w = 1$, and a carrier wavelength of 2π . The accuracy of the DP code has been checked by several researchers. Among these, the recent study by [Skyner \(1996\)](#) compared numerical predictions from the DP code with subsurface velocity measurements made during the breaking onset process using particle image velocimetry techniques. After a small shift of the numerical data to match the surface profiles, the predicted and measured kinematics were in close (within 2%) agreement. The predicted and measured surface shapes were also in very close agreement. From such studies, the essential features of two-dimensional wave breaking appear to be captured by the DP code well into the overturning regime and conclusions drawn from studying the model behavior are likely to be relevant to the actual fluid dynamics underlying the onset of wave breaking in self-modulating wave groups. Most of the computations reported in this paper are based on the DP code.

For the chirped wave packet (case III) calculations, in which the leading waves have a higher frequency than trailing waves, we used a fully nonlinear numerical model developed by Y. Agnon and N. Drimer (1998, personal communication) with refinements by A. Segre (1998, personal communication). This code (henceforth referred to as the DAS code) solves the fully nonlinear, irrotational free surface boundary value problem using the boundary element method within a numerical wave channel, featuring a piston wave maker at one end of the domain and an energy absorbing “beach” at the other end. This code is capable of representing wave surfaces past the point of overturning, that is, beyond a vertical forward face configuration, without numerical smoothing. Drimer and Agnon (1998, personal communication) document a number of error validation tests. Their computed surface profiles were in close agreement with previous results of [Jansen \(1986\)](#) and [New et al. \(1985\)](#) for steep sinusoidal waves. The wave height versus water depth curve obtained by Drimer and Agnon agrees well with the experimental results of [Hansen and Svendsen \(1979\)](#) for wave shoaling up to breaking. We also checked the accuracy of their model in our present computations by verifying global conservation of water volume and total energy after the piston motion ceases. In all cases that we checked, errors both in wave energy and volume remained smaller than 2% during the subsequent wave propagation.

b. Model runs

A series of runs using the DP code was performed in this study. To eliminate the effects of numerical instabilities and obtain a stable solution in our calculations, following BT, we chose in the DP model a small precision control parameter $\epsilon = 0.001$, fifth-order backward differencing, the number of points per wave $NP = 16$ with no numerical smoothing. We took the still water depth $h = 50$ and used a time step of $0.1T$, where $T = 2\pi$ for all calculations with the DP code. Two classes of initial wave group structures, cases I and II defined below, were used in our DP code runs.

A number of maximally recurrent and breaking wave realizations for case III wave packets were also studied using the DAS code. These runs all started from a still water initial state. A time step of $0.05T$ was used for all calculations with the DAS code, where T is the reference input period of the piston movement. The number of points along the boundary was chosen to provide the desired channel geometry and resolution of the overturning wave profile. We tested various values of NP on the boundary, especially on the free surface, and found that taking $NP = 20$ was sufficiently large to ensure a stable result. Zero artificial damping coefficient was used for all the DAS computations. The piston was stopped after the wave group had built up, allowing a chirped wave packet to propagate in the positive x direction.

c. Initial wave group structures

Three classes of initial wave group structures were investigated in this study. The first class (henceforth referred to as case I) had a fundamental carrier wave with two small symmetric sidebands, using as parameters the initial carrier wave amplitude a_0 (or steepness $s_0 = a_0 k_0$, where $k_0 = 1$) and the number of waves in one modulation length, N . The initial wave group had the structure of a uniform, steady, finite amplitude deep water wave train whose linear approximation is $\eta = a_0 \cos(k_0 x)$, where $k_0 = 1$. On this primary wave are superimposed perturbations having the initial form

$$\begin{aligned} & \varepsilon a_0 \cos\left(\frac{N+1}{N}k_0x - \theta\right) \\ & + \varepsilon a_0 \cos\left(\frac{N-1}{N}k_0x - \theta\right) \\ & \text{with } \varepsilon = 0.1 \quad \text{and} \quad k_0 = 1. \end{aligned} \quad (1)$$

Here, N is the integer number of waves in the group, where $3 \leq N \leq 10$. This is the range used by DP and provides sideband perturbation wavenumbers in the range [0.667, 1.333]. Also, following DP, the phase angle θ was taken as $\pi/4$ as it provides the most rapid initial growth of the sideband modes.

The second class of wave groups (henceforth referred to as case II) had an initial bimodal spectrum of the form

$$\begin{aligned} \eta &= a_0 \cos(k_0x) \\ & + \varepsilon a_0 \cos\left(\frac{N+1}{N}k_0x - \frac{\pi}{18}\right) \\ & \text{with } \varepsilon = 1 \quad \text{and} \quad k_0 = 1, \end{aligned} \quad (2)$$

where a_0 and N are as defined as above. The small phase shift, retained from BT, is inconsequential.

A third class of wave group structures (henceforth referred to as case III) had a more rapidly deforming geometry and was characterized as a ‘‘chirped’’ wave packet. This structure, commonly implemented in wave tank experiments (e.g., RM), comprises carrier waves that coalesce rapidly due to their different phase velocities. These wave packets were produced in the DAS code by driving the piston wave maker with the motion

$$\begin{aligned} x_p &= -0.25A_p \left(\tanh\frac{4\omega_p t}{N\pi} + 1 \right) \\ & \times \left[1 - \tanh\frac{4(\omega_p t - 2N\pi)}{N\pi} \right] \sin \left[\omega_p \left(t - \frac{0.018t^2}{2} \right) \right], \end{aligned} \quad (3)$$

where t is time and N is a integer that controls the number of waves produced by the piston, A_p is proportional to the piston amplitude and

$$\omega_p = \sqrt{g \frac{2\pi}{\lambda} \tanh\left(\frac{2\pi}{\lambda}h\right)}$$

is its angular frequency, λ is the wavelength, and h is the still water depth. To simulate deep water, we took the still water depth near the piston as $h = 4$ with $\lambda = 2$.

3. Properties of nonlinear wave group evolution

a. Evolution to recurrence or breaking

The transition between evolution with recurrence or evolution to breaking occupies a position of central importance in the discussion of breaking criteria. In this context, both model studies and laboratory investigations have typically investigated initial value problems and have adopted a measure based on the initial carrier wave steepness to parameterize their results. This choice of initial steepness parameter warrants discussion, especially as various investigators have reported appreciably

different initial steepness thresholds that separate recurrence from breaking cases.

In their study of weak sideband modulating case I wave groups, DP used the initial amplitude a and wavenumber k of the center Fourier mode to characterize the initial steepness $(ak)_0$ of their wave groups and found that this initial steepness threshold for breaking onset depends on the number of carrier waves N in the group, ranging from $(ak)_0 = 0.150$ for $N = 3$ to $(ak)_0 = 0.088$ for $N = 10$.

The DP definition of initial steepness requires modification in the context of a full wave modulation (our case II) that results from the superposition of two modes of equal, moderate steepness with a prescribed wavenumber separation. There are two straightforward options for specifying a characteristic initial steepness measure. The first uses the root mean square (rms) steepness

$$(ak)_0^{\text{rms}} = \left[\sum_{i=1}^{N_0} (a_i k_i)^2 \right]^{1/2} \quad (4)$$

for a free surface specified by the Fourier series $\eta(x, t) = \sum_{i=1}^{N_0} a_i \cos(k_i x - \omega_i t - \phi_i)$. In (4), a_i , k_i , ω_i , and ϕ_i are, respectively, the amplitude, the wavenumber, the frequency, and the phase of the i th component, and N_0 is the number of wave components.

The second initial steepness measure, introduced by RM in their laboratory study of chirped wave packets, defines a spectrally based initial wave steepness ak_c as

$$ak_c = \left(\sum_{n=1}^{N_c} a_n \right) k_c = \frac{1}{4} \left(\sum_{n=1}^{N_c} a_n \right) (\sqrt{k_1} + \sqrt{k_{N_c}})^2, \quad (5)$$

where a_n and k_n are the Fourier amplitudes ($1 \leq n \leq N_c$) of their initially uniform spectral amplitude wave packet, assuming a linear dispersion relation between temporal and spatial variations. Rapp and Melville showed that the energy loss associated with breaking events was well correlated with this parameter.

For cases I and II, the differences in using these two definitions are shown in Fig. 3a. The chirped wave (case III) data from RM shows a threshold level of $ak_c \sim 0.25$, yet the rms steepness threshold is typically only 0.055. Thus the critical value of ak_c for breaking not only depends on the number of carrier waves, N , in the group but also on the initial group structure, suggesting its unsuitability as a threshold parameter for characterizing the onset of wave breaking. We conclude that neither of these initial steepness measures provides a consistent, robust indicator for breaking onset.

Finally, we point out that the perturbations imposed on the initial wave group geometry were all in the initially unstable regime. It is of interest to note how the recurrence/breaking margin for different N relate to the theoretical loci of the most unstable *initial* sideband perturbations (e.g., see Tulin and Waseda 1999, Fig. 1). This comparison is shown on a plot of initial center steepness versus relative bandwidth for case I wave groups in Fig. 3b. This suggests a nonsimple relationship between the *initial* sideband instability growth rate and the *ultimate* onset of recurrence or breaking.

b. Evolution characteristics

The complex evolution characteristics for the wave elevation and local energy density shown in Figs. 1–3 and related issues such as breaking onset, timing, and strength are among many fascinating aspects of this problem that motivated our present investigation into whether these processes might be determined by an intrinsic “universal” threshold parameter. In an earlier paper by the second author, BT, it was found that, if the local mean wave energy density or wave action density is used to characterize the evolution of these nonlinear wave groups, the implicit averaging over even a single carrier wavelength loses the spatial localization of the energy maximum. To address this basic issue, BT adopted wave energy and momentum densities averaged locally over one-half of the carrier wavelength as the primary variables, as these variables and their rates of change appeared to have reasonably well-localized maxima. A fundamental result reported by BT was that the envelope maxima of these densities fluctuate on a “fast” timescale, about twice the carrier wave period. This is linked to the well-known crest–trough asymmetry of steep gravity waves and a close analog of this behavior is shown in Fig. 5 below in the context of a more detailed discussion on its origin. Banner and Tian also reported that the corresponding relative growth rates following their envelope maxima have a substantial dynamic range. For a range of case I wave groups containing different numbers of waves, they reported finding a common threshold behavior for the maximum value of either

of these local relative growth rates that determined whether breaking subsequently occurred.

c. BT revisited

The breaking onset criterion proposed by BT was based on the behavior on the fast timescale described above. This led to the conclusion that breaking onset could be detected only within less than one-half of the mean carrier wave period. We decided to revisit this important issue, as well as related concerns such as possible sensitivity of the results to other initial wave group geometries, to certain numerical approximations that were made and to the temporal resolution of the BT analysis. To address these goals, we developed an intrinsically more accurate numerical methodology based on a “wave group following” (henceforth WGF) computational approach that allowed us to calculate, with minimal filtering and numerical approximation, the entire “slow” evolution of the energetics of the wave group, as well as the “fast” evolution.

This method underpinned our efforts to understand at what point during the evolution the wave group is destined to proceed irreversibly to break and its connection with the mean energy convergence rate toward the envelope maximum highlighted in [Figs. 1](#) and [2](#). It also allowed a detailed assessment of the BT methodology and conclusions, which is reported in appendix A. From this assessment, we concluded that

1. while the half-wavelength average adopted by BT had good localization properties for the envelope maximum and its rate of change, our WGF analysis revealed that this averaging masked the difference between breaking and recurrent cases through a subtle smearing of the behavior of the envelope maximum;
2. the envelope maximum migrates between the steepest crest to the steepest trough in a complex fashion, implying that the BT assumption of a constant value of the velocity c_E of the energy envelope maximum is not justified.

Making this assumption can lead to significant errors in calculating energy growth rates following the envelope maximum using the Eulerian expression $\partial/\partial t + c_E \partial/\partial x$. These difficulties are avoided using our WGF approach.

These results convinced us that the complex details are smoothed to such an extent even with half-wavelength averaging that only a *local* quantity is able to provide a clear resolution of the differences between breaking and recurrence cases. Therefore in the present paper, we focused on the behavior of the depth-integrated local energy density at its maximum along the wave group, as defined in the following section. Rather than working in terms of the dimensional wave energy, we investigated the behavior of a dimensionless measure of the mean maximum local energy density and its dimensionless growth rate, as defined in the following section. This growth rate was then calculated systematically using a WGF technique that allowed us to investigate the entire growth cycle with no additional approximations and negligible filtering.

Aside from the intrinsically improved accuracy, the present calculations extend significantly the scope of those described by BT to the wider class of initial wave group geometries, as described above. In addition, [Banner and Song \(2002\)](#), hereafter Part II) reports the results of our investigation of the influence of wind forcing and a typical background vertical shear current on the evolution to breaking for many typical cases.

As described below, the behavior of our proposed dimensionless growth rate parameter reveals a robust common threshold for all routes to breaking for all the deep water wave cases we have examined, providing an earlier and more decisive indicator for the onset of breaking than previous criteria. It also appears to reflect the relative strength of breaking events.

d. Diagnostic growth rate parameter

Based on the preceding discussion on the WGF technique, we chose a *local*, nonhorizontally averaged measure of the wave energy at its maximum along the wave group as the basis of a diagnostic parameter that could distinguish between breaking and recurrence evolution. We used the depth-integrated local wave energy density $E(x; t)$, given by the sum of kinetic and potential energy contributions of the fluid particles along the vertical line at x at time t :

$$E(x; t) = \int_{-h}^{\eta} \frac{1}{2} \rho_w (u^2 + v^2) dy + \frac{1}{2} \rho_w g \eta^2, \quad (6)$$

where u and v are the x and y velocity components, g is gravitational acceleration, ρ_w is the density of water, h is the still water depth, and $y = \eta(x, t)$ is the free surface elevation.


Following BT, for these irrotational flows the interior velocity field (u, v) was calculated from the boundary values using Green's theorem and then used to calculate the local energy $E(x; t)$ in [\(6\)](#) for cases I and II. For case III, E could be obtained directly from the code output. The behavior of E at specific times during the evolution for each case was shown in

In order to provide “global” criteria, we needed to introduce suitable nondimensional parameters for E and its growth rate following the energy maximum of the wave group. We explored the possibility of using the dimensionless relative local energy growth rate

$$\frac{1}{\omega E} \frac{DE}{Dt},$$

but found that this parameter did not provide a robust indicator for resolving the onset of breaking or recurrence for the ensemble of cases we studied.



We investigated two other nondimensional parameters based on E . One was E normalized by the mean energy $\langle E_T \rangle$ of the wave group. For cases I and II, $\langle E_T \rangle$ is conserved for unforced calculations or is easily calculated at different stages of evolution when wind input is added. The chirped wave packet (case III) presents the only complication for this approach. While the total packet energy is conserved during unforced evolution, the spatial spreading is unbounded. This presents conceptual difficulties in relation to providing a mean energy level for comparison with oceanic cases. Excluding this case, $\langle E_T \rangle$ can provide a useful normalization.

Other suitable diagnostic parameters based only on local wave train properties were the parameters $s = (E/(\rho_w g))^{1/2} k$ or $s^2 = [E/(\rho_w g)] k^2$. For these, the local wavenumber k was calculated systematically from the x derivative of the unfolded phase function computed from the Hilbert transform of the free-surface profile. Following BT (section 2.3.4 and Fig. 6 ) , suitable low-pass filtering was applied using a bidirectional Butterworth filter determined by the requirement for a smooth distribution of the local wavenumber along the wave profile. Extensive testing indicated that even for extreme waves just prior to breaking, the calculated wavenumber after filtering was within 5% of the mean of the physical wavenumbers determined from the wave profile by direct measurement of successive crests, troughs, and zero-crossings.

The diagnostic parameters s and s^2 provide measures of local wave steepness without the complication of dealing with issues such as waveform asymmetry. At the instantaneous location x_{\max} of the maximum of s^2 along the wave group, the corresponding value s_{\max}^2 reflects the square of the maximum local steepness of the carrier waves. The choice of s_{\max}^2 rather than s_{\max} circumvented the need to investigate locally large values of $D s_{\max}/Dt$, which occurred even for modest values of s_{\max} due to intrinsic local unsteadiness in the evolution of the extrema of s_{\max} and are clearly not related to the onset of breaking or recurrence, for which the values of s_{\max} need to be large as well. Use a diagnostic growth rate based on $D s_{\max}^2/Dt$ weights $D s_{\max}/Dt$ by the magnitude of s_{\max} , thereby linking maxima of $D s_{\max}/Dt$ with the larger values of s_{\max} appropriate to breaking or recurrence. Accordingly, we adopted $\mu = s_{\max}^2$ as our preferred diagnostic parameter and investigated its evolution. From this, we calculated the evolution of its local average value $\langle \mu \rangle$ and the corresponding dimensionless growth rate

$$\delta = \frac{1}{\omega_c} \frac{D}{Dt} \langle \mu \rangle,$$

for the various cases, where ω_c is the initial mean carrier wave frequency. The detailed methodology for computing $\langle \mu \rangle$ and δ is described in appendix B.

As was already seen in Figs. 1  and 2 , nonlinear deep water wave group modulation has an associated *mean* convergence of energy toward the energy maximum. These figures indicate that most of the change in μ is associated with wave energy density changes, with a much smaller contribution arising from changes in k^2 . On this basis, $\langle \mu \rangle$ and δ could be regarded as surrogate parameters reflecting the resultant of this complex energy flux process. The results of this approach are described in detail in the following section. We conclude by noting that, for periodic boundary condition cases, the alternative nondimensional parameter based on energy $E/\langle E_T \rangle$ suggested above showed very similar properties for forecasting breaking onset and might be more straightforward to measure in open ocean applications.

4. Scope of the present WGF calculations

a. Growth rate computations

We investigated the behavior of $\mu(t)$, $\langle\mu(t)\rangle$, and $\delta(t)$ at each time step as the wave group evolved. For any given time t during the evolution, from the local energy $E(x; t)$ and wavenumber $k(x; t)$, we calculated $\mu = s^2(x_{\max}; t)$ at the location x_{\max} of the maximum of s^2 and hence determined its local average (see [section 4b](#) below) and nondimensional local average growth rate $\delta(t)$. Further, we verified that, if we chose instead to track this quantity either at the maximum of the wave envelope (calculated from the Hilbert transform of the free surface) or at the maximum surface displacement $[\eta]_{\max}$, the results for $\delta(t)$ were virtually identical.

Typical evolution curves of $\mu(t)$, $\langle\mu(t)\rangle$, and $\delta(t)$ are shown in [Fig. 4](#) for case I wave groups just below and above their recurrence threshold. It is seen that the recurrence cases attain their greatest value of $\delta(t)$ well before $\mu(t)$ reaches its recurrence maximum, where $\delta(t) = 0$.

Also, in the evolution of $\mu(t)$, a fast oscillation with period $2T$ is seen to be superimposed on the longer term evolution growth toward the recurrence maximum or breaking onset. This is due to the strong crest/trough asymmetry of steep nonlinear gravity waveforms shown in the fast evolution sequence of [Fig. 5](#). This figure shows the strong contrast in E for the two times separated by T when the crest and trough occupy the envelope maximum of $\mu(x; t)$.

b. The mean growth rate

Based on the clear indication of mean convergence of wave-coherent energy at the energy maximum of the group seen in [Figs. 1](#), [2](#), and [4](#), we propose that

1. it is the average growth rate $\delta(t)$ that represents the mean convergence rate of wave energy at the energy maximum within the group;
2. this growth rate is a fundamental determinant of recurrence or breaking;
3. the fast $O(2T)$ oscillatory component of $\mu(t)$ associated with the kinematics of the asymmetric wave profile is not the primary determinant of recurrence/breaking.

To filter out the rapid fluctuations superimposed on the longer-term trend, we used a method based on smoothed spline fitting that was superior to conventional filtering techniques in regard to managing the end effects at the onset of breaking. Details describing the technique and its accuracy are given in appendix B, but we note that the same “tolerance” parameter in the smoothed spline fitting was used to calculate $\delta(t)$ for all wave group cases (I, II, and III) and that the results were insensitive to the choice of this parameter ranging over two orders of magnitude.

For completeness, examples of case II and case III evolution are shown in [Figs. 6](#) and [7](#). The greater initial modulation depth of case II is seen to provide a more rapid evolution to recurrence or breaking near the recurrence threshold than the comparable case I results shown in [Fig. 4](#). This appears to be associated with its stronger initial local energy distribution contrast within the wave group. The case III evolution is seen to be faster than cases I or II, underlying its popularity in laboratory experiments (e.g., RM).

Systematic computations of $\mu(t)$, $\langle\mu(t)\rangle$, and $\delta(t)$ were carried out for a range of N and initial steepness levels for each of the three cases I, II, and III. Our aim was to investigate

1. whether recurrence and breaking could be robustly linked to a threshold behavior of $\delta(t)$ and, if so, at what stage of the evolution was the onset of breaking determined;
2. whether the strength of breaking events could be related to the magnitude of $\delta(t)$ just preceding breaking onset. This inference was based on the conceptual link between $\delta(t)$ and the mean convergence rate (or accumulation rate) of energy at the energy maximum, and hence to the rate at which the breaking crest needed to dissipate the accumulated energy in excess of the maximum accumulation rate corresponding to the recurrence limit.

5. Results

a. Existence of a common threshold for breaking

[Figs. 4](#), [6](#), and [7](#) show typical long-term evolution curves of $\mu(t)$, $\langle\mu(t)\rangle$, and $\delta(t)$ for each of the three different initial group cases. They reveal distinctly different generic evolution curve behavior for the recurrence cases and similarly

for the breaking cases.

For breaking cases, the diagnostic growth rate $\delta(t)$ increases continually until breaking occurs, while for recurrence cases, $\delta(t)$ initially increases, then ceases growing at the peak of $\mu(t)$, and then begins decreasing. Our results show that this behavior does not depend sensitively on the number of waves N in the group. [Table 1](#) summarizes the key results of our long-term evolution calculations for different wave group lengths N for the three cases I, II, and III. These results include the time t_{th} when $\delta(t)$ attains the upper bound of the breaking onset threshold range δ_{th} , as discussed in detail below; the time of breaking onset t_{br} and the corresponding growth rate $\delta(t_{br})$, or the time of the recurrence peak (t_{max}) and the corresponding maximum growth rate $\delta(t_{gr,max})$.

It is interesting to note that the evolution time to breaking differs markedly, both within each of the cases I, II, and III for different N and between the various cases for the same N . The evolution time correlates with the *initial* degree of departure of the wave group structure from spatial uniformity and on the number of waves in the group. Also, the growth rate evolution curves for $\delta(t)$ show varying degrees of smoothness, with case II evolution curves typically showing more intrinsic variability.

On the fundamental question of predicting the onset of breaking or recurrence, reference to [Table 1](#) shows that the maximum growth rate δ^{max} can clearly distinguish breaking from recurrence for any particular case. For example, $\delta^{max} = 0.83 \times 10^{-3}$ for the maximally recurrent case I wave group with $N = 5$ and initial steepness $(ak)_0 = 0.111$ while for the comparable marginal breaking case with initial steepness $(ak)_0 = 0.112$, $\delta^{max} = 1.93 \times 10^{-3}$. However, from this table it is also seen that δ^{max} shows considerable variation among each of the different cases investigated and hence does not provide a *unique* breaking threshold. Despite considerable effort, we were unable to find an alternative parameter that could provide a unique threshold.

Nevertheless, our results in [Table 1](#) show that the maximum value δ^{max} of the growth rate $\delta(t)$ can be used as the basis of a *common* threshold parameter that clearly distinguishes recurrence cases from breaking cases and does not depend on the group structure or number of waves N in the group or the type of initial wave group structure. Based on the ensemble of results for the three different classes of initial wave group geometry (cases I, II, and III) in [Table 1](#), we propose that a common growth threshold δ_{th} for breaking can be taken within the range 1.30×10^{-3} to 1.50×10^{-3} . Breaking is seen to occur whenever $\delta(t)$ exceeds δ_{th} , while the maximum values of $\delta(t)$ for all of the recurrence cases remains below δ_{th} . This key aspect of our findings is summarized graphically in [Fig. 8](#).

b. Time between exceeding threshold and breaking onset

Foreshadowing the results of Part II, it is found that the same proposed threshold range for δ_{th} is valid in the presence of wind forcing and a background shear current. Further, supplementary results on the influence of intermediate water depth on breaking onset, to be reported elsewhere, indicate that choosing δ_{th} at the upper boundary 1.50×10^{-3} also embraces unforced intermediate water depth propagation in mean water depths of up to at least one-third of the mean wavelength. On this basis, we decided to use $\delta_{th} = 1.50 \times 10^{-3}$ as the reference level for assessing other properties of interest, such as the lead time between exceeding the threshold and breaking onset, noting that this choice provides the most conservative estimate of the lead time t_{lead} .

It is evident from [Table 1](#) that each case has a different time interval t_{lead} between when the nominal threshold $\delta_{th} = 1.50 \times 10^{-3}$ is exceeded and the actual onset of breaking. Some cases break within a short time, comparable to half the carrier wave period, while other cases break only after more than four carrier wave periods have elapsed. To our knowledge, this is the first systematic assessment of the lead time to breaking.

c. Breaking strength

It is observed that individual waves break with varying intensities, often characterized from “spilling” to “plunging,” yet there is presently little quantitative understanding of what controls this observed variation in breaking strength. Rapp and Melville investigated this question observationally in their extensive laboratory study of chirped wave packets, quantifying the relative or energy loss as the change in wave energy density (energy per unit width of the flow for 2D waves) before and after breaking, normalized by the energy density prior to breaking. They explored how this parameter varied as a function of their initial wave steepness parameter ak_c for different wave packet geometries, such as relative bandwidth and distance to

breaking, we found that their breaking intensity, for conditions ranging from plunging breaking waves, correlated strongly with the initial wave steepness parameter ak_c . The trend of their results is shown in [Fig. 9](#).

For comparison, [Fig. 10](#) shows our computed evolution curves for $\langle\mu(t)\rangle$ and the derived dependence on ak_c of δ^{\max} for case III wave groups with $N = 5$, for initial steepness levels for marginal recurrence and a number of breaking cases with progressively larger ak_c . While this approach is unable in principle to provide absolute levels of energy loss fraction, we see its value as potentially supporting our viewpoint that it is the mean energy convergence rate to the group maximum that underlies the onset and strength of breaking. Indeed, the favorable correspondence with the observational results in [Fig. 9](#) both with respect to the general shape and threshold initial steepness provide encouraging initial support for our proposed association of breaking strength with δ^{\max} preceding breaking onset.

For comparison, [Figs. 11](#) and [12](#) show the trend of the calculated results similar to [Fig. 10](#), but for case I and II wave groups with $N = 5$. The overall trends are not dissimilar, but the marginal breaking steepness ak_c thresholds are significantly reduced while the levels of δ^{\max} are very similar. These differences warrant further observational investigation, especially as it has not been established whether chirped wave studies are representative of ocean wave breaking.

[Table 2](#) summarizes the maximum growth rate estimates and associated parameters of interest for cases I, II, and III for a range of N values. In all cases, δ^{\max} is found to increase with initial wave steepness while the corresponding breaking time t_{br} decreases rapidly. In addition, from the data for case I, the trend of δ^{\max} with ak_c is shown in [Fig. 13](#) and suggests an appreciable dependence of predicted breaking strength on the number of waves N in the group. Results for case II seen in [Fig. 14](#) show a similar dependence, but for a more limited range of N . This potentially interesting influence of group size on predicted breaking strength could be investigated in future observational studies.

6. Conclusions

Determining whether breaking will occur within a two-dimensional nonlinear modulating wave group evolving in deep water has been investigated in numerical experiments in terms of the behavior of a diagnostic dimensionless growth rate associated with the energy maximum of the wave group. Two different fully nonlinear, two-dimensional inviscid free surface codes were used in our computations and many initial wave group structures were analyzed. In this paper we introduced the conceptual framework and investigated conservative (unforced) nonlinear wave group evolution. In Part II, we report on the additional influences of wind forcing and a background shear current on the evolution to breaking of the wave group.

The major conclusions of the present study are then as follows:

1. Both for breaking and recurrence, the local energy and its growth rate following the wave group maximum evolves in a complex fashion, with a fast oscillation superimposed on a longer term mean trend. We propose that it is the longer term trend, which reflects a systematic mean energy convergence toward (or away from) the maximum energy region within the wave group, that determines the ultimate breaking or recurrence behavior. The fast oscillation, due to the strong crest/trough asymmetry of the carrier waves, is believed to be primarily a kinematic effect.
2. Our calculations indicate that breaking or recurrence may be determined by a common threshold δ_{th} in the range $(1.30 \times 10^{-3}, 1.50 \times 10^{-3})$ for the nondimensional growth rate $\delta(t)$ of the proposed diagnostic parameter $\langle\mu(t)\rangle$, independent of the initial group structure. For the various cases investigated, recurrence always occurred when the maximum value of $\delta(t)$ attained a peak value below this threshold level, after which it decreased. This is in contrast with all breaking cases we investigated, where $\delta(t)$ continued to increase after it reached this threshold level, after which breaking always occurred subsequently within a time interval ranging from a fraction to several carrier wave periods.

Foreshadowing the results of Part II, the same breaking threshold range for δ_{th} is found to be applicable to all cases of wind forcing, vertical shear wind-driven and combinations of these cases that we investigated. Further, choosing δ_{th} at the upper bound 1.50×10^{-3} allows the inclusion of flat bottom cases for mean water depths at least as shallow as one-third of the mean wavelength.

3. We propose that the strength of breaking events is related to the mean rate of convergence of energy at the group maximum immediately preceding breaking onset and is reflected by the corresponding value of $\delta(t)$ at $t = t_{break}$. The

trend of our calculations of $\delta(t_{\text{break}})$ for periodic nonlinear wave groups shows an encouraging close qualitative correspondence with laboratory measurements of the fractional mean energy loss associated with breaking waves for increasing initial group steepness.

4. The new insight into the breaking process provided by these numerical experiments warrants a detailed observational investigation to establish the validity of the proposed threshold and indicative breaking strength properties of the diagnostic parameter $\delta(t)$.

Acknowledgments

The authors gratefully acknowledge the financial support of the Australian Research Council for this project. We also sincerely thank Prof. D. H. Peregrine, Prof. J. W. Dold, and Prof. Y. Agnon for allowing us to use their numerical codes.

REFERENCES

- Banner M. L., and D. H. Peregrine, 1993: Wave breaking in deep water. *Annu. Rev. Fluid Mech.*, **25**, 373–397. [Find this article online](#)
- Banner M. L., and X. Tian, 1998: On the determination of the onset of wave breaking for modulating surface gravity water waves. *J. Fluid Mech.*, **367**, 107–137. [Find this article online](#)
- Banner M. L., and J. B. Song, 2002: On determining the onset and strength of breaking deep water waves. Part II: Influence of wind forcing and surface shear. *J. Phys. Oceanogr.*, **32**, 2559–2570. [Find this article online](#)
- Boccotti P., G. Barbaro, and L. Mannino, 1993: A field experiment on the mechanics of irregular gravity waves. *J. Fluid Mech.*, **252**, 173–186. [Find this article online](#)
- Dias F., and C. Kharif, 1999: Nonlinear gravity and capillary-gravity waves. *Annu. Rev. Fluid Mech.*, **31**, 301–346. [Find this article online](#)
- Dold J. W., and D. H. Peregrine, 1986: Water-wave modulation. *Proc. 20th Int. Conf. on Coastal Engineering*, Taipei, Taiwan, ASCE, 163–175.
- Donelan M. A., and W. H. Hui, 1990: Mechanics of ocean surface waves. *Surface Waves and Fluxes*, G. L. Geernaert and W. J. Plant, Eds., Vol. 1, Kluwer, 209–246.
- Donelan M. A., M. S. Longuet-Higgins, and J. S. Turner, 1972: Whitecaps. *Nature*, **239**, 449–451. [Find this article online](#)
- Dysthe K. B., 1979: Note on a modification to the nonlinear Schrödinger equation for application to deep water waves. *Proc. Roy. Soc. London*, **A369**, 105–114. [Find this article online](#)
- Griffin O. M., Coauthors, 1996: Kinematic and dynamic evolution of deep water breaking waves. *J. Geophys. Res.*, **101**(C7), 16515–16531. [Find this article online](#)
- Hansen J. B., and I. A. Svendsen, 1979: Regular waves in shoaling water experimental data. Institute of Hydrodynamics and Hydraulic Engineering, Technical University of Denmark Series Paper No. 21, 20 pp. and 213 pp. of appendixes.
- Holthuijsen L. H., and T. H. C. Herbers, 1986: Statistics of breaking waves observed as whitecaps in the open sea. *J. Phys. Oceanogr.*, **16**, 290–297. [Find this article online](#)
- Jansen P. C. M., 1986: A boundary element model for non-linear free surface phenomena. Delft University of Technology Rep. No. 86-2, 39 pp.
- Kway J. H. L., Y.-S. Loh, and E.-S. Chan, 1998: Laboratory study of deep-water breaking waves. *Ocean Eng.*, **25**, 657–676. [Find this article online](#)
- Longuet-Higgins M. S., 1984: Statistical properties of wave groups in a random sea state. *Philos. Trans. Roy. Soc. London*, **A312**, 219–250. [Find this article online](#)
- Melville W. K., 1982: The instability and breaking of deep-water waves. *J. Fluid Mech.*, **115**, 165–185. [Find this article online](#)
- Melville W. K., 1983: Wave modulation and breakdown. *J. Fluid Mech.*, **128**, 489–506. [Find this article online](#)
- Melville W. K., 1996: The role of surface-wave breaking in air–sea interaction. *Annu. Rev. Fluid Mech.*, **26**, 279–321. [Find this article online](#)

- Nepf H. M., C. H. Wu, and E. S. Chan, 1998: A comparison of two- and three-dimensional wave breaking. *J. Phys. Oceanogr.*, **28**, 1496–1510. [Find this article online](#)
- New A. L., P. McIver, and D. H. Peregrine, 1985: Computations of overturning waves. *J. Fluid Mech.*, **150**, 233–251. [Find this article online](#)
- Osborne A. R., M. Onorato, and M. Serio, 2000: The nonlinear dynamics of rogue waves and holes in deep-water gravity wave trains. *Phys. Lett.*, **A275**, 386–393.
- Phillips O. M., D. Gu, and M. A. Donelan, 1993: Expected structure of extreme waves in a Gaussian Sea. Part 1. Theory and SWADE buoy measurements. *J. Phys. Oceanogr.*, **23**, 992–1000. [Find this article online](#)
- Rapp R. J., and W. K. Melville, 1990: Laboratory measurements of deep water breaking waves. *Philos. Trans. Roy. Soc. London*, **A331**, 735–800. [Find this article online](#)
- Skyner D., 1996: A comparison of numerical predictions and experimental measurements of the internal kinematics of a deep-water plunging wave. *J. Fluid Mech.*, **315**, 51–64. [Find this article online](#)
- Tulin M. P., and J. Li, 1992: On the breaking of energetic waves. *Int. J. Offshore Polar Eng.*, **2**, 46–53. [Find this article online](#)
- Tulin M. P., and T. Waseda, 1999: Laboratory observations of wave group evolution, including breaking effects. *J. Fluid Mech.*, **378**, 197–232. [Find this article online](#)

APPENDIX A

7. Refinement of the BT98 Calculations

In the course of our investigation, we reviewed certain key aspects of the BT analysis. The following findings led to the refinements that were central to the present study.

A number of approximations were made by BT in calculating the nondimensional relative growth rate parameters for $\hat{E}_{1/2}$ and $\hat{M}_{1/2}$ following the wave envelope maximum. In particular, BT estimated these growth rates through the Eulerian operator

$$\frac{D\hat{E}_{1/2}}{Dt} = \frac{\partial\hat{E}_{1/2}}{\partial t} + c_{\hat{E}_{1/2}} \frac{\partial\hat{E}_{1/2}}{\partial x},$$

discussing in some detail the potential sources of error in this approach. After implementing our more direct WGF method, we noted the following:

1. BT found that $c_{\hat{E}_{1/2}} \sim 0.75$ at selected times during the evolution and adopted this as a constant for all times. We found that within a cycle of $O(2T)$, $c_{\hat{E}_{1/2}}$ actually varied quite markedly and we were concerned that the assumption of constant $c_{\hat{E}_{1/2}}$ may have led to errors in their calculations of the growth rate $\beta^{\max}_{\hat{E}_{1/2}}(t)$.
2. BT needed to use smoothing (postfiltering) in their calculations. We were concerned about the overall influence of this filtering although BT reported that their results were not sensitive to the choice of filter properties.
3. We noted a minor coding error that caused $\hat{E}_{1/2}$ to be underestimated by several percent, although this may have only had a secondary effect on the results since this term appears in normalized form in the growth rate.

We undertook a systematic investigation to assess the impact of these potential sources of error. After correcting the coding error in the BT calculation of the local wave energy (and momentum density), we investigated the errors caused by filtering and the assumption that $c_{\hat{E}_{1/2}}$ had a fixed value of 0.75. We recalculated the relative growth rate of $\beta^{\max}_{\hat{E}_{1/2}}(t)$ as defined in BT by our more accurate explicit WGF technique. These calculations showed that the maximum of $\beta^{\max}_{\hat{E}_{1/2}}(t)$

for the marginal breaking case is just a little larger than for the marginal recurrence, without an obvious threshold separating these cases. This agrees with BT, but we could not reproduce the subsequent near-constant positive growth rate reported by BT after the threshold was reached. Our assessment of the likely source of error follows below.

Although $c_{\hat{E}_{1/2}}$ is close to the surface envelope velocity $c_{se} = 0.5$ for linear wave groups, our detailed WGF calculations revealed that both $c_{\hat{E}_{1/2}}$ and c_{se} could not be taken as a constant. Rather, they both have rapid fluctuations due to the highly asymmetric carrier wave profiles that characterize the evolution of nonlinear wave groups. [Figure A1](#) shows the fluctuations of c_{se} and $c_{\hat{E}_{1/2}}$ for case I with $N = 5$ and $(ak)_0 = 0.12$ during the time interval $(58.5, 60.5)$. The largest values (near the phase speed $c = 1$) was found both for c_{se} and $c_{\hat{E}_{1/2}}$, when the much sharper and higher crest occupies the envelope maximum, as seen in [Fig. A2](#). The smallest values (sometimes less than zero) occur both for c_{se} and $c_{\hat{E}_{1/2}}$ when the trough is at the envelope maximum, as seen in [Fig. A3](#).

To minimize the errors arising from the assumption that $c_{\hat{E}_{1/2}}$ has a constant value of 0.75 and from filtering, we recalculated the relative growth rate of $\beta_{\hat{E}_{1/2}}^{\max}(t)$ defined in BT by using the following simple WGF derivative

$$\beta_{\hat{E}_{1/2}}^{\max} = \frac{\hat{E}_{1/2}^{\max}(t + \Delta t) - \hat{E}_{1/2}^{\max}(t - \Delta t)}{2\omega\Delta\hat{E}_{1/2}^{\max}(t)},$$

where $\hat{E}_{1/2}^{\max}(t)$ is $\hat{E}_{1/2}$ evaluated at the envelope maximum at time t . This intrinsically more accurate approach highlighted the absence of any obvious threshold apparent between the marginal recurrence and the marginal breaking cases. Moreover, it motivated our present focus on $\mu(t)$ and on the longer term evolution $\langle\mu(t)\rangle$ as the correct physical basis for breaking onset.

APPENDIX B

8. Calculations of $\langle\mu(t)\rangle$ and δ^{\max}

The local average of $\mu(t)$, denoted $\langle\mu(t)\rangle$, was calculated using standard MATLAB software. A few methods were tested to find a robust method for evaluating the mean (or the trend) using various analytical test signals and the calculated data. Serious difficulties can occur near the ends where the data have large oscillations when using polynomial fitting, bidirectional filtering with standard Butterworth or Chebyshev filters, or wavelet analysis methods. To reduce the end effects as far as possible, the method used in this paper was to

1. detect the local maximum points and minimum points of $\mu(t)$;
2. fit cubic smoothing splines to the respective sets of detected maximum and minimum points over the whole time interval. For these calculations, we used the MATLAB routine “spaps.m” with a tolerance $TOL = 10^{-7}$ and uniform weights $W = 1/N_r$, where N_r is the total number of points in the ensemble. TOL could be varied between 10^{-6} and 10^{-8} with no significant change to the results;
3. obtain the local average $\langle\mu(t)\rangle$ as the average of the smooth-splined maximum and minimum curves.

A typical example is illustrated in [Fig. B1](#), which shows $\mu(t)$ and the corresponding $\langle\mu(t)\rangle$ for maximally recurrent and marginal breaking case I wave groups with $N = 5$.

The diagnostic growth rate function $\delta(t)$ was routinely calculated by differentiating $\langle\mu(t)\rangle$ using centered differences, with backward differences for the last time step. The maximum value δ^{\max} was detected using the MATLAB library routine *max*. For breaking cases, the occurrence of δ^{\max} at the endpoint of the growth curve for $\langle\mu(t)\rangle$ required special attention. The calculation of δ^{\max} depends on the numerically challenging task of determining a derivative at the endpoint of an interval of a heavily smoothed oscillatory function. Issues such as the spatial resolution of the surface and the temporal resolution of the

time-stepping each had an effect on the endpoint of the calculation just prior to breaking and hence on the value of δ^{\max} . These effects were of secondary importance in relation to our primary goal of determining a breaking onset criterion, but need to be noted in relation to the proposed link between δ^{\max} and breaking intensity.

The results presented were based on standard time steps of $0.1T$ for cases I and II, and $0.05T$ for case III used in our calculations of $\mu(t)$, $\langle\mu(t)\rangle$, and the average growth rate $\delta(t)$. For recurrence cases, the influence of a smaller time step or higher spatial resolution on the calculations was negligible. However, for breaking cases, using a smaller time step can allow the evolution of the wave group to proceed marginally further before breaking onset and these additional values of $\mu(t)$ can have a small influence on $\langle\mu(t)\rangle$ and, hence, affect the value of δ^{\max} at breaking onset. We explored the effect of increasing the spatial resolution and found that increasing spatial resolution had little impact on our calculated values of δ^{\max} at breaking onset. We also routinely examined visually the wave profile and local energy for the last time step prior to breaking onset to check for smoothness. In only very few cases was there evidence of nonsmoothness, in which case we discarded this point.

Overall, with smaller time steps of $0.01T$ we found typical increases of $O(25\%)$ for δ^{\max} at breaking onset and that the absolute level of δ^{\max} at breaking onset can only increase. On this basis we concluded that our standard resolution results are on the conservative side in supporting our proposed breaking onset criterion. In regard to the proposed link between δ^{\max} at breaking onset and breaking strength, the effect of increased resolution would preserve the overall trend of our results but rescale the ordinate by $O(25\%)$. Since the comparison we make is qualitative, this has no significant impact on our conclusion. In any event, with the potential sensitivity of these results to the method used to filter $\mu(t)$ to obtain $\langle\mu(t)\rangle$, it is essential that these numerical results be investigated through careful measurements. Such a companion observational laboratory program is presently in progress.

Tables

TABLE 1. Summary of the maximum growth rates and key time scales from the numerical experiments for the three cases I, II, and III with zero forcing: δ^{\max} is the maximum growth rate; t_{br} is the time of breaking onset; t_{th} is the time when the growth rate $\delta(t)$ reaches the upper bound of the breaking threshold band $\delta_{th} = 1.50 \times 10^{-3}$; t_{max} and $t_{gr,max}$ are the times of the recurrence peak and the corresponding maximum growth rate; $t_{lead} = t_{br} - t_{th}$ is the lead time between $\delta(t)$ exceeding the breaking threshold δ_{th} and the time of breaking onset; s_0 is the initial carrier wave steepness; A_p is proportional to the piston amplitude; N is the number of waves in the group; T is the carrier wave period, R stands for recurrence, and B denotes breaking

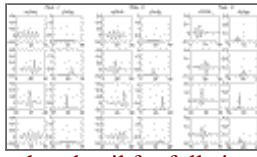
Cases	N	s_0	A_p	t_c (w/ t_{max})	t_c (w/ $t_{gr,max}$)	t_{br}	$\delta^{\max} \times 10^3$
I (R)	3	0.150	—	54.97	57.57	—	0.69
I (R)	5	0.111	—	54.25	55.57	1.37	2.30
I (R)	5	0.111	—	66.37	82.77	—	0.83
I (R)	5	0.112	—	80.37	80.87	0.57	1.93
I (R)	7	0.099	—	80.47	96.77	—	0.75
I (R)	7	0.100	—	90.37	95.7	0.77	2.12
I (R)	8	0.095	—	102.37	105.87	—	0.92
I (R)	8	0.096	—	101.27	107	0.87	2.22
I (R)	10	0.088	—	1137	1267	—	0.84
I (R)	10	0.089	—	1287	126.87	0.67	1.62
II (R)	3	0.079	—	21.47	23.47	—	1.23
II (R)	5	0.060	—	21.27	23.57	2.37	1.60
II (R)	5	0.069	—	30.97	43.87	—	0.99
II (R)	5	0.070	—	37.77	40.37	2.57	2.81
II (R)	8	0.058	—	62.97	67.37	—	0.96
II (R)	8	0.059	—	64.87	67.67	2.87	1.68
II (R)	10	0.054	—	81.37	85.77	—	0.88
II (R)	10	0.055	—	81.57	82.47	0.97	1.97
III (R)	5	—	0.035	10.67	24.67	—	0.97
III (R)	5	—	0.036	16.67	18.97	2.37	2.76
III (R)	8	—	0.028	29.67	39.7	—	0.93
III (R)	8	—	0.029	26.97	31.37	4.47	2.28

Click on thumbnail for full-sized image.

TABLE 2. Maximum growth rates and key time scales for selected breaking case I, II, and III wave groups for different initial steepness s_0 and different N . Symbols in this table have the same meanings as in Table 1

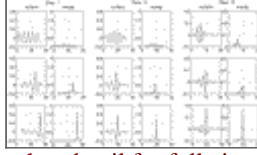
Cases	N	A_p	s_0	t_c	t_c	t_c	$\delta^{\max} \times 10^3$
I (B)	3	—	0.151	54.2	55.57	0.77	3.009
I (B)	5	—	0.160	27.37	34.77	2.57	4.18
I (B)	5	—	0.180	20.07	24.37	4.37	7.85
I (B)	5	—	0.200	12.67	16.27	3.67	8.75
I (B)	5	—	0.112	80.37	80.87	0.57	1.93
I (B)	5	—	0.120	56.17	60.37	4.47	3.27
I (B)	5	—	0.140	26.57	40.47	3.07	5.31
I (B)	5	—	0.160	27.17	30.67	3.57	6.75
I (B)	5	—	0.180	26.27	24.67	4.47	7.16
I (B)	5	—	0.200	19.27	15.97	4.77	9.49
I (B)	5	—	0.070	27.77	40.27	2.57	2.80
II (B)	5	—	0.060	23.77	26.77	3.07	5.61
II (B)	5	—	0.090	15.67	19.27	3.67	6.80
II (B)	5	0.056	—	16.67	18.97	2.37	7.75
III (B)	5	0.038	—	10.67	14.57	3.17	5.27
III (B)	5	0.060	—	9.27	12.37	3.67	7.35
III (B)	5	0.042	—	7.87	10.47	2.67	7.55
III (B)	5	0.064	—	5.87	8.47	2.67	7.79
I (B)	7	—	0.100	94.37	957	0.67	2.12
I (B)	7	—	0.110	68.17	70.67	2.77	6.26
I (B)	7	—	0.130	47.37	50.97	3.67	8.51
I (B)	7	—	0.150	36.17	39.47	3.17	11.57
I (B)	7	—	0.170	28.17	31.67	3.57	11.65
I (B)	7	—	0.190	22.77	26.27	3.57	12.36
II (B)	7	—	0.062	57.17	60.37	3.27	1.73
II (B)	7	—	0.070	27.67	41.37	3.07	4.88
II (B)	7	—	0.080	28.07	31.67	3.67	6.54
II (B)	7	—	0.090	19.17	24.17	3.07	7.97
II (B)	7	—	0.100	16.07	18.87	2.87	8.65
II (B)	7	—	0.110	12.27	15.07	3.47	9.51
I (B)	10	—	0.088	119.57	119.57	1.07	1.96
I (B)	10	—	0.100	97.27	94.37	3.07	4.20
I (B)	10	—	0.110	75.47	80.47	5.07	9.14
I (B)	10	—	0.130	56.87	60.97	4.17	10.95
I (B)	10	—	0.150	48.87	49.47	3.67	13.61
I (B)	10	—	0.170	38.87	40.37	3.67	16.65
I (B)	10	—	0.190	30.87	34.57	3.77	16.74

Click on thumbnail for full-sized image.



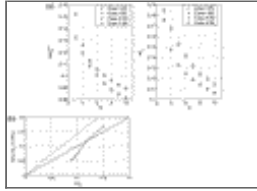
[Click on thumbnail for full-sized image.](#)

FIG. 1. Surface profiles (left-hand panels) (axes show lengths in meters) and the corresponding local energy distributions (right-hand panels) (in J m^{-1}) at selected times during the evolution of the three marginally stable initial wave group cases (I, II, and III) containing N carrier waves, where $N = 5$. For case I the initial steepness parameter $s_0 = 0.111$ and the selected times from top to bottom are, respectively, $t/T = 0, 60, 82.7,$ and 160.5 , where T is the reference carrier wave period. For case II the initial steepness parameter $s_0 = 0.069$ and the selected times from top to bottom are, respectively, $t/T = 0, 30, 43.8,$ and 98.4 . For case III the initial piston amplitude parameter $A_p = 0.035$, the wavelength $\lambda = 2$, and the selected times from top to bottom are, respectively, $t/T = 7.5, 20, 25.6,$ and 47.5



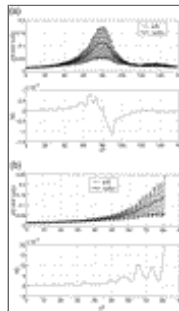
[Click on thumbnail for full-sized image.](#)

FIG. 2. As for [Fig. 1](#) but for marginally breaking cases. For case I the initial steepness parameter $s_0 = 0.112$ and the selected times from top to bottom are, respectively, $t/T = 0, 60,$ and 80.8 . For case II the initial steepness parameter $s_0 = 0.070$ and the selected times from top to bottom are, respectively, $t/T = 0, 30,$ and 40.2 . For case III the initial piston amplitude parameter $A_p = 0.036$, the wavelength $\lambda = 2$, and the selected times from top to bottom are, respectively, $t/T = 7.5, 15,$ and 18.9



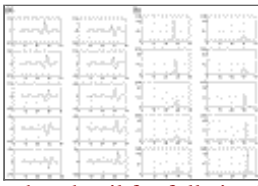
[Click on thumbnail for full-sized image.](#)

FIG. 3. (a) The dependence on the number of waves N in the group of the initial wave steepness at the margin between recurrence and breaking for case I and II wave groups. (left) Based on the rms steepness; (right) uses the initial steepness measure ak_c based on the Fourier modes (see [section 3a](#)). The symbols are in the legend. (b) Locus of maximally recurrent initial perturbations (solid-star curve) plotted in the initial perturbation steepness-relative bandwidth plane, in relation to the most unstable *initial* perturbation characteristics (solid line) for case I wave groups. The dashed line is the classical Benjamin–Feir stability boundary. Here the initial carrier wave steepness $(ak)_0 = a_0 k_0$, a_0 is the initial carrier wave amplitude, $k_0 = 1$, $\omega_0 = (gk_0)^{1/2}$, $\omega_{\pm} = ([(N+1)/N] gk_0)^{1/2}$, and $3 \leq N \leq 10$



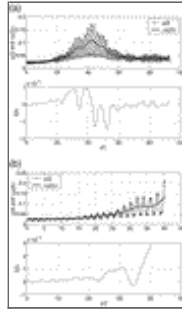
[Click on thumbnail for full-sized image.](#)

FIG. 4. Long-term evolution (a) of the parameter $\mu(t)$ and its local average $\langle \mu(t) \rangle$ (heavy continuous line) for the marginal recurrence case I with $N = 5$ and $s_0 = 0.111$. The lower panel shows the corresponding nondimensional growth rate $\delta(t)$. (b) As for (a) but for the marginal breaking case I with $N = 5$ and $s_0 = 0.112$



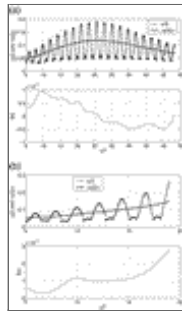
Click on thumbnail for full-sized image.

FIG. 5. (a) The short-term evolution of the surface elevation profile for case I with $N = 5$ and $s_0 = 0.112$ for the interval t/T from 79.0 to 80.8 in increments of 0.2, with time increasing vertically downward in each panel. (left panels) Starting from $t/T = 79.0$ and (right panels) starting from $t/T = 80.0$. (b) Corresponding spatial distributions of the diagnostic local wave steepness parameter s^2 defined in [section 3d](#) for the surface profiles and evolution times in [Fig. 5a](#)



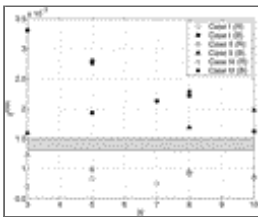
Click on thumbnail for full-sized image.

FIG. 6. As in [Fig. 4](#) but for (a) the marginal recurrence case II for $N = 5$ and $s_0 = 0.069$ and (b) the marginal breaking case II for $N = 5$ and $s_0 = 0.070$



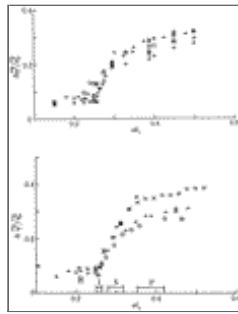
Click on thumbnail for full-sized image.

FIG. 7. As in [Fig. 4](#) but for (a) the marginal recurrence case III with piston amplitude parameter $A_p = 0.035$ and (b) for the marginal breaking case III with piston amplitude parameter $A_p = 0.036$



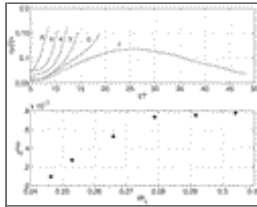
Click on thumbnail for full-sized image.

FIG. 8. Summary of all results for the maximum nondimensional growth rate δ^{\max} for case I, II, and III wave groups as a function of the number of waves N in the wave group. The marginal recurrence and marginal breaking results are shown, respectively, with open and dark symbols and the legend identifies the cases. The proposed breaking onset threshold δ_{th} for deep water waves lies within the shaded band



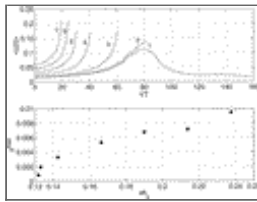
Click on thumbnail for full-sized image.

FIG. 9. Observed loss of excess momentum flux against ak_c for (top) five packet bandwidths and (bottom) three center packet frequencies. Incipient breaking, spilling, and plunging breaking events are marked I, S, P, respectively. After [Rapp and Melville \(1990\)](#)



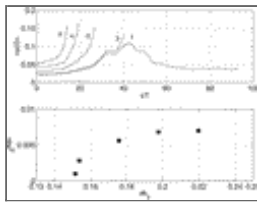
Click on thumbnail for full-sized image.

FIG. 10. Mean evolution of the local average nondimensional parameter $\langle \mu(t) \rangle$ and the associated maximum growth rate δ^{\max} for breaking cases of different initial steepness for case III with $N = 5$. (top) The numbers on the curves correspond to different values of the initial piston amplitude parameter A_p as follows: 1 ($A_p = 0.035$), 2 ($A_p = 0.036$), 3 ($A_p = 0.038$), 4 ($A_p = 0.040$), 5 ($A_p = 0.042$), 6 ($A_p = 0.044$)



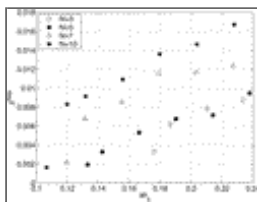
Click on thumbnail for full-sized image.

FIG. 11. As in [Fig. 10](#) but for case I with $N = 5$. (top) The numbers on the curves in the upper panel correspond to different initial steepness values s_0 as follows: 1 ($s_0 = 0.111$), 2 ($s_0 = 0.1125$), 3 ($s_0 = 0.12$), 4 ($s_0 = 0.14$), 5 ($s_0 = 0.16$), 6 ($s_0 = 0.18$), and 7 ($s_0 = 0.20$)



Click on thumbnail for full-sized image.

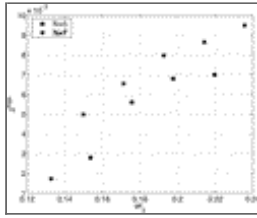
FIG. 12. As in [Fig. 10](#) but for case II with $N = 5$. The numbers on the curves in the upper panel correspond to different initial steepness values s_0 as follows: 1 ($s_0 = 0.069$), 2 ($s_0 = 0.07$), 3 ($s_0 = 0.08$), 4 ($s_0 = 0.09$), and 5 ($s_0 = 0.10$)



Click on thumbnail for full-sized image.

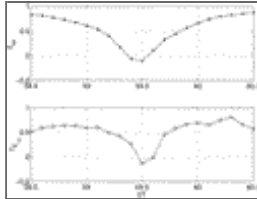
FIG. 13. Maximum nondimensional growth rates δ^{\max} for breaking case I wave groups as a function of initial wave steepness for different numbers of waves in the group for $N = 3, 5, 7$, and 10 . The symbols corresponding to the different N are identified in

the legend



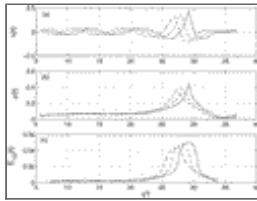
Click on thumbnail for full-sized image.

FIG. 14. Maximum nondimensional growth rates δ^{\max} for breaking case II wave groups as a function of initial wave steepness for different numbers of waves in the group for $N = 5$ and 7 . The symbols corresponding to the different N are identified in the legend



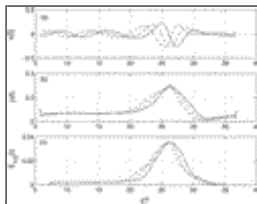
Click on thumbnail for full-sized image.

FIG. A1. Propagation speeds of (top) the surface envelope maximum c_{se} and (bottom) the half-wavelength averaged energy $c_{\hat{E}_{1/2}}$ for the case I wave group with $N = 5$, $s_0 = 0.12$ during the time interval $t/T = 58.5-60.5$



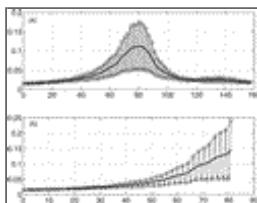
Click on thumbnail for full-sized image.

FIG. A2. The surface profile $\eta(t)$, surface envelope $\rho(t)$, and half-wavelength averaged energy $\hat{E}_{1/2}$ for the case I wave group with $N = 5$, $s_0 = 0.12$ at $t/T = 60$ (dashed line), 60.2 (dash-dotted line), and 60.4 (solid line). For these times, the crest is at the envelope maximum



Click on thumbnail for full-sized image.

FIG. A3. As for Fig. A2 but at times $t/T = 59.3$ (dashed line), 59.5 (dash-dotted line), and 59.7 (solid line) when the trough is at the envelope maximum



Click on thumbnail for full-sized image.

FIG. B1. The open circles joined by solid lines show the results of the cubic smooth spline fit to the local maxima and minima of $\mu(t)$ and the thick solid line shows $\langle \mu(t) \rangle$, the average of these two smooth spline curves. (a) Marginal recurrence case I wave group with $N = 5$ and $s_0 = 0.111$. (b) Marginal breaking case I wave group with $N = 5$ and $s_0 = 0.112$

Corresponding author address: Dr. Michael L. Banner, School of Mathematics, The University of New South Wales, Sydney 2052, New South Wales, Australia. E-mail: m.banner@unsw.edu.au

top ▲



© 2008 American Meteorological Society [Privacy Policy and Disclaimer](#)

Headquarters: 45 Beacon Street Boston, MA 02108-3693

DC Office: 1120 G Street, NW, Suite 800 Washington DC, 20005-3826

amsinfo@ametsoc.org Phone: 617-227-2425 Fax: 617-742-8718

[Allen Press, Inc.](#) assists in the online publication of *AMS* journals.